A Cost-Efficient Data-Driven Approach to Design Space Exploration for Personalized Geometric Design in Additive Manufacturing

SungKu Kang[1]
Data Science and Visualization Laboratory,
Department of Industrial and Systems Engineering,
Virginia Tech,
Blacksburg, VA 24060
e-mail: kangsungku@vt.edu

Xinwei Deng
Associate Professor
Department of Statistics,
Virginia Tech,
Blacksburg, VA 24060
e-mail: xdeng@vt.edu

Ran Jin
Associate Professor
Data Science and Visualization Laboratory,
Department of Industrial and Systems Engineering,
Virginia Tech,
Blacksburg, VA 24060
e-mail: jran5@vt.edu

Additive manufacturing (AM) is considered as a key to personalized product realization as it provides great design flexibility. As the flexibility radically expands the design space, current design space exploration methods for personalized geometric designs become time-consuming due to the use of physically based computer simulations (e.g., finite element analysis or computational fluid dynamics). This poses a significant challenge in design for an efficient personalized product realization cycle, which imposes a tight computation cost constraint to timely respond to every new requirement. To address the challenge, we propose a cost-efficient data-driven design space exploration method for personalized geometric design in AM, enabling feasible design regions under the computation constraint. Specifically, the proposed method adopts surrogate modeling of efficient voxel model-based design rules to identify feasible design regions considering both manufacturability and personalized needs. Since design rules take much less time for evaluation than physically based simulations, the proposed method can contribute to timely providing feasible design regions for an efficient personalized product realization cycle. Moreover, we develop a cost-based experimental design for surrogate modeling, which enables the evaluation of additional design points to provide more precise feasible design regions under the computation cost constraint. The merits of the proposed method are elaborated via additively manufactured microbial fuel cell (MFC) anode design. [DOI: 10.1115/1.4050984]

Keywords: computational foundations for additive manufacturing, computer aided design, data-driven engineering

1 Introduction

Additive manufacturing (AM) allows unprecedented design freedom in manufacturing a large variety of parts with complex geometric structures [1]. Therefore, AM is considered as the key to popularizing personalized product, so that every product can be highly optimized to a specific personalized need or special functionality. A motivating example is designing a personalized anode structure for a microbial fuel cell (MFC), which has been intensively studied to harvest electricity from wastewater through bio-electrochemical reactions [2]. Specifically, to achieve optimal performance, the MFC anode structure should be personalized to maximize the performances (e.g., power density) in specific waste water treatment conditions. First, the overall geometric shape of MFC anode will be tailored according to the chamber design. The requirements on power density, operating condition (e.g., seawater), and/or the necessity of stack-ability [3] call for different chamber designs, which involves the decisions on MFC chamber design, such as tubular type, flat plate type, and H-shaped type. Second, the cavity size of the MFC anode should be optimized according to the operating condition of the MFC. Typically, a smaller cavity size is preferred to provide a larger surface area for bio-electrochemical reactions, but too small cavity size could result in clogginess to impact the long-term operability of a MFC [4]. The feasible range of cavity size is related to the materials selected for the anode structure and the bacteria types. For example, when a bamboo charcoal tube is used as the electrode material, it is reported that the cavity size is preferred to be larger than 2 mm to prevent clogginess after a long-term operation [5]. On the other hand, it is known that a certain combination of bacteria species and anode material (e.g., Geobacter species and gold electrode) form thicker bio film (i.e., requires larger cavity), while another combination (e.g., Shewanella species and gold electrode) does not form biofilm at all (i.e., allowing smaller cavity) [6]. Thus, different operating condition necessitate the personalization of MFC anode structure not only in terms of the overall shape but also in terms of internal anode structure.

In the context, AM is regarded as a promising option to fabricate a personalized MFC anode as it can provide personalized geometry with a high surface-volume ratio for optimal performance [7,8]. However, to fully take advantage of the potential of AM in popularizing personalized products, it is necessary to timely identify an optimal geometric design for every new personalized need, which imposes a tight computation cost constraint in design space exploration.

Therefore, an efficient design exploration method is needed for timely identifying feasible design regions conforming to a personalized need, especially within a tight computation cost constraint. However, as AM's design freedom has radically expanded the design space, design space exploration relying on physically based simulations (e.g., finite element analysis or computational fluid dynamics) typically takes too much time, which results in the computation bottleneck to the efficient exploration of the product design [9,10]. For example, in the case of the motivating example, it is necessary to simulate the biofilm build-up on the MFC anode surface to identify potential clogginess after a long-term

[1]Corresponding author.

Contributed by the Computers and Information Division of ASME for publication in the Journal of Computing and Information Science in Engineering. Manuscript received June 11, 2020; final manuscript received April 16, 2021; published online May 14, 2021. Assoc. Editor: Yong Chen.

operation, which takes too much time (e.g., at least several hours per each run) to timely explore the design space [11]. In the context, efficient exploration of the design space for AM, especially applicable to a tight computation cost constraint, is an important catalyst to popularize personalized product realization via AM.

Providing an efficient design space exploration for personalized geometric design, which is applicable to a tight computation cost constraint, is important due to the following advantages. First, an efficient design space exploration can address the design bottleneck, which is not feasible with design space exploration relying on physically based computer simulations. Second, a design space exploration method, designed to provide feasible design regions within a tight computation cost constraint, will provide a practical mechanism to enable efficient personalized product realization in a wide variety of application domains. Third, a design space exploration method capable of supporting personalized geometric design will provide a quantitative method to evaluate how design variables and process parameters interact with the manufacturability and conformance to personalized needs. In other words, addressing the design bottleneck for the personalized geometric design for AM will contribute to popularizing personalized product realization, and thus open a wide variety of new opportunities. However, existing design methods are not suitable to satisfy the needs of timely delivering personalized geometric design for AM.

To support the design process tailored for AM, a new family of methods called design for additive manufacturing has been studied. In terms of geometric design, optimization-based design is receiving much attention as AM affords extensive design freedom. Specifically, the methods utilize iterative topology optimization to derive an unconventional optimal design, which is enabled via AM's design flexibilities [12–14]. However, it is extremely challenging to timely explore a comprehensive design space (i.e., the design space incorporates both design variables and process parameters) with physically based simulations, especially in the case of multi-physics applications [15] similar to the motivating example. To address the issue, some design approaches consider avoiding comprehensive physically-based simulations, such as procedural design via homogenization of stochastic foam structure [16]. However, such method cannot easily control local features, and they may not applicable to general product design where local features need to be well controlled (e.g., for MFC anode, local cavity size should be carefully controlled to prevent clogginess). Also, as existing optimization-based designs do not properly consider user needs and the interaction between design variables and process parameters yet [9], they are not suitable to support personalized design for AM in a timely manner. On the other hand, some of the existing works have tried extending conventional Design for Manufacturing (DfM) for AM by employing design for manufacturing rules. Specifically, efficient mechanisms to evaluate design constraints related to layer-wise AM, such as minimum feature size, overhang angle, and surface roughness, have been developed to identify the manufacturability of the arbitrary design. For example, voxel model-based implementation of design rules [17] and heat kernel signature-based implementation of design rules [18] have been proposed for the efficient implementation of design for manufacturability. While the methods provide a relatively more efficient method to evaluate the feasibility of a design, the methods have not translated the feasibility into a quantitative design space incorporating both design variables and process parameters, nor considered translating user needs into quantitative design rules. In the meantime, a few studies have investigated the application of data-driven methods to support design for AM, including the use of Bayesian network classifiers [19] and Gaussian process regression model [20] for design space exploration. Even though data-driven methods seem promising to speed up the design process to support timely personalized product realization, the existing works still do not properly consider personalized needs [19] or still require physically based simulations for metamodeling [20], which limit their applications to timely deliver personalized product realization.

In short, current optimization-based design and design space exploration methods are not sufficiently efficient to satisfy a tight computation cost constraint due to the computation cost of physically based computer simulations. Moreover, even though the interaction between design variables/process parameters and personalized needs are important considerations, the existing methods do not properly consider such needs in design space exploration. Such a lack of efficient design space exploration for the personalized geometric design for AM seems to limit AM's capability to popularize personalized product realization.

To address the challenges, we propose a cost-efficient data-driven design exploration method in the personalized geometric design for AM, which can efficiently provide tailored feasible regions to facilitate the follow-up design exploitation (e.g., more detailed simulation-based exploration or design optimization). Specifically, the proposed design exploration method relies on the surrogate modeling of efficient design rules and the cost-based experimental design, founded on a quantitative design space incorporating both design variables and process parameters. The proposed method has three steps. First, a quantitative design space for AM is proposed, which is built upon the combination of bottom-up design strategy and voxel modeling to incorporate both design variables and process parameters. Specifically, the bottom-up design strategy allows a small number of design variables to define the overall geometry with a lattice structure, and voxel modeling allows AM process parameters (e.g., layer thickness) to represent the overall geometry with as-fabricated voxel model [21]. Second, using efficient voxel model-based design rules, the distribution of feasibility-related features are timely derive via surrogate modeling. It should be noted that the feasibility-related features include the features related to the manufacturability (e.g., minimum feature size) and conformance to personalized needs (e.g., MFC anode cavity size) to incorporate personalization in design space exploration. In surrogate modeling, we propose the cost-based experimental design that adaptively favors design points with lower evaluation costs while maintaining space-filling-ness as possible. Lastly, a set of thresholds, which is based on domain knowledge, are applied to the distributions of the feasibility-related feature to identify feasible/infeasible design regions over the design space.

There are four major contributions of the proposed method. First, the proposed method provides a quantitative design space for AM incorporating both design variables and process parameters. Therefore, it provides the foundation of quantifying the correlation between design variables/process parameters and manufacturability/conformance to personalized needs. Second, as the proposed design space can uniquely represent each geometric design via as-fabricated voxel model, the proposed method can systematically implement efficient design rules regarding manufacturability and personalized needs via simple Boolean and algebraic operations (e.g., counting the number of consecutive voxels to estimate feature size). As the evaluation of the design rules takes at most several minutes, this ensures the efficiency of the proposed method, such that it can effectively facilitate the follow-up design exploitation. Third, as the proposed experimental design allows an additional number of design points within the same computation cost constraint, it contributes to providing more precise feasible design regions especially when a tight cost constraint is applied. Lastly, the proposed method can be easily extended to a wide variety of applications involving layer-wise AM processes without much modifications and applicable to various domains when relevant design rules are available. For example, one can obtain the manufacturability rules on stereolithography [22] and dimensioning/selection rules on prosthesis design [23,24] and apply the proposed method in prosthetic hand design for additive manufacturing. Similarly, the design rules on printed electronics [25] can be acquired to apply the proposed method to facilitate personalized foldable/rollable electronics design [26]. Combined with automated rule extraction frameworks [27], such design rules can be efficiently acquired from unstructured text with minimal

intervention of domain experts. The proposed method facilitates the design exploitation by significantly narrowing down the entire design space into feasible design regions. Hence, it can address various types of practical design problems when coupled with the existing works on design space mapping for reconfigurable and flexible systems [28–31]. In summary, the proposed method can address the computation bottleneck and systematically incorporate manufacturability and personalized needs via efficient design rules and is capable of providing feasible design regions within a tight computation cost constraint. The proposed method can be applied to the personalized geometric design for systems where adopting a lattice structure is beneficial. Since lattice structures are being actively adopted to achieve a wide variety of mechanical/thermal/electrical properties (e.g., high strength-to-weight ratio, high energy absorption, and thermal insulation) [21], the proposed method can contribute to realizing the effective personalized product realization cycle in many different applications, such as the personalized geometric design of a lightweight prosthesis conforming to patients' anatomy.

The remainder of this paper is organized as follows. In Sec. 2, we review the existing work on design space exploration. In Sec. 3, we detail the proposed design space exploration method by highlighting surrogate modeling via voxel model-based design rules and cost-based experimental design. In Sec. 4, the proposed method is applied to personalized MFC anode design as a case study. Finally, we will provide our conclusions and discuss the future work in Sec. 5.

2 State-of-the-Art

Design space exploration refers to the procedure to identify all feasible design alternatives satisfying a set of requirements (e.g., performance requirements and manufacturability). Specifically, the main objective of design space exploration to identify the boundary between feasible and infeasible designs [20]. In this section, the existing design space exploration methods are reviewed, and the challenges in the methods are presented. Based on the literature, existing design space exploration methods can be categorized into two types: exhaustive search and statistical inference.

Exhaustive search approach first divides a design space into a set of hypercubes and then evaluates design samples in the hypercubes via computer simulations or physical experiments. In exhaustive search approach, the boundary between feasible and infeasible designs is usually expressed in an explicit way, such as intervals of design variables or via visualization tools. The examples of the exhaustive search approach include inductive design exploration method proposed by Choi et al. [32] and surrogate-assisted illumination method proposed by Morris et al. [19]. However, exhaustive search approach requires the evaluation of too many designs to identify precise boundaries, which makes the approach not suitable for the comprehensive design space provided by AM.

On the other hand, statistical inference approach first evaluates a relatively smaller number of design samples and then a probabilistic model is used to identify the boundary between feasible and infeasible designs. In statistical inference approach, the boundary between feasible and infeasible designs can also be represented in an implicit way, such as classification models. Statistical inference approach can be further classified based on the type of probabilistic model used for design space exploration. For example, Matthews et al. and Shahan et al. demonstrated the method based on Bayesian network classifier [33,34], and Chen and Fuge presented the method based on Gaussian process classifier [35]. Also, a recent approach utilized both of Bayesian network classifier and Gaussian process regression [20] to improve the classification performance. However, as the methods still rely on computer simulations or physical experiments, it is too time-consuming, thus not able to timely address the needs for the personalized design. Moreover, for the personalized design for AM, computer simulation cost becomes more demanding, as the simulation may involve multi-physics simulation for complex shapes.

Existing design space exploration methods are not suitable to timely deliver personalized design for AM in a comprehensive design space incorporating design variables and process parameters. Thus, there is a need for an efficient design space exploration method, which can timely support personalized design. To address the challenge, we demonstrate an efficient data-driving design space exploration method that utilizes surrogate models of efficient design rules. Also, we propose the cost-based experimental design, which can provide more precise feasible design regions within a tight computation cost constraint for the efficient personalized product realization cycle.

3 Proposed Method

3.1 Overview. Figure 1 shows an overview of the proposed design exploration method (top), with the main contributions of the proposed method marked as bold, along with its overall system informatics (bottom). The proposed method is suitable for systems with the assumption that (1) adopting a lattice structure is beneficial to identify optimal designs via AM (e.g., when a lightweight geometric design is desired) and (2) reliable design rules related to manufacturability and personalized functionality exist. When the aforementioned assumptions hold, the proposed method is applicable to many different systems (e.g., prosthetic hand design). The system informatics provides the digital foundation of the proposed method. In the system informatics, it is shown that a set of design variables and process parameters (x_1 to x_p) defines a CAD model with a lattice structure, and then the CAD model is converted into a voxel model to enable the derivation of feasibility-related features (e_1 to e_q) via voxel model-based design rules. The features include manufacturability-related features (e.g., minimum feature size) and personalized needs-related features (e.g., cavity size for bamboo charcoal MFC anode). Next, a set of feasibility threshold values based on the design rules (e.g., "minimum feature $\geq$2 mm" or "MFC anode cavity size $\geq$2 mm") are applied to e_1–e_q to derive binary feasibility indicators (z_1 to z_q). Lastly, the overall feasibility (y) of the design is derived from the interaction of z_1 to z_q. Given the system informatics, the proposed design exploration methods translate the process of identifying the feasibility of designs into a quantitative design space through the following steps: defining quantitative design space, surrogate modeling of design rules, and identifying feasible design regions.

Step 1. Defining quantitative design space: In this step, a set of design variables and AM process parameters are used to define a quantitative design space providing the foundation of design space exploration.

Step 2. Surrogate modeling of design rules: In this step, a set of design rules are identified, and the voxel model-based implementations of the design rules are used to evaluate feasibility-related features. Then, the cost-based experimental design is used to construct surrogate models of the design rules which generate the distribution of the feasibility-related features across the design space.

Step 3. Identifying feasible design regions: In this step, a set of feasibility threshold values (based on domain knowledge) are applied to the distribution of the feasibility-related features to identify the distribution of binary feasibility indicators across the design space. Then, the intersection of the distribution yields feasible design regions, which provide the significantly narrowed down design space for efficient design exploitation.

3.2 Quantitative Design Space. The objective of this step is to define a quantitative design space that incorporates design variables and process parameters directly affecting geometric design.

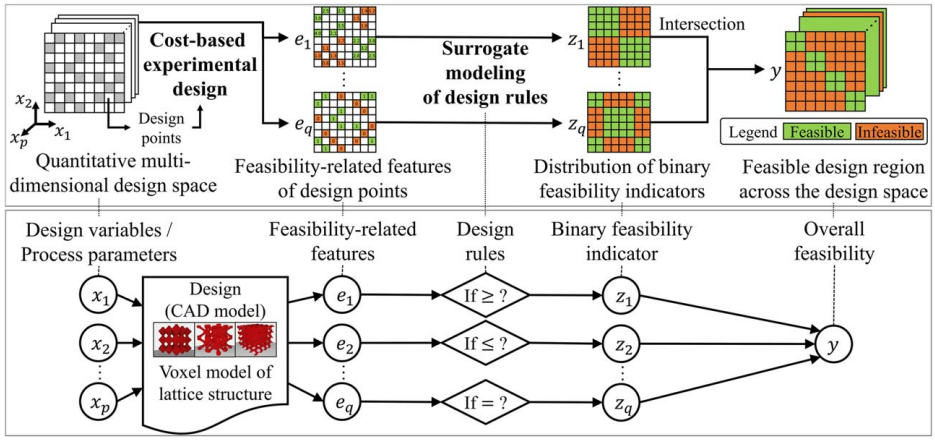

Fig. 1 An overview of the proposed method (top), with the main contributions of the proposed method marked as bold, along with its overall system informatics (bottom)

Figure 2 shows how the design space is defined. Specifically, we first adopt a bottom-up design strategy to define a complex lattice structure with a set of design variables, and then translate the structure into a voxel model to reflect a more realistic shape from layer-wise AM process based on a set of process parameters. As we focus on geometric design, the process parameters not directly affecting geometric design (e.g., extrusion temperature, printing speed) are not incorporated.

3.2.1 Bottom-Up Design Strategy. Lattice structure has been widely adopted to maximize AM's capability, as it provides superior properties (e.g., strength-to-mass ratio, surface-to-volume ratio) not obtainable with conventional manufacturing processes [36]. For example, lattice structure has been adopted to design additively manufactured MFC anodes in several pieces of literature, due to its good surface-to-volume ratio [7,8,37]. In this context, we adopt the bottom-up design strategy to define the geometric shape of a design with a lattice structure, as shown in the top-left of Fig. 2. First, the type of generic unit cell is chosen from the unit cell library. The examples of unit cell type include triply periodic minimal surface (TPMS)-based unit cells [38] or octet-truss unit cells [39]. Second, the properties of the unit cell are chosen to define its specific shape. For TPMS-based unit cell, unit cell size and volume fraction can be controlled as shown in Fig. 2. Once the design variables (i.e., unit cell type and properties) are chosen, they represent a uniquely defined lattice structure. In case that the design may have different sizes, the overall dimension can be also added as design variables to represent the design space. The advantage of the approach is that a lattice structure with complex geometry can be uniquely represented with a relatively smaller number of quantitative design variables, compared to other freeform object representations.

3.2.2 Voxel Representation. Once the design variables are chosen, the overall geometric shape of a design is defined. However, in the case of layer-wise AM processes including fused filament fabrication (FFF), the actual printed shape may be slightly different from the theoretical shape, due to the "staircase effect" [21,40]. In the context, we convert the lattice structure into as-fabricated voxel model [21] to provide more realistic representations of designs. Specifically, we control the voxel shape with a set of process parameters (i.e., voxel height is the same as layer thickness) and control the voxel organization with other sets of process parameters (i.e., the geometric shape is rotated based on a given build orientation before translated into a voxel model) as shown in bottom-left of Fig. 2. As a result, by combining the design variables and process parameters (center of Fig. 2), we define a quantitative multi-dimensional design space, so that each design point uniquely defines the as-fabricated voxel model of a specific lattice structure (right side of Fig. 2). In addition, as-fabricated voxel model enables an intuitive way to derive design features via simple Boolean and algebraic operations (i.e., simply counting the number of corresponding voxels). Even though other representations such as the signed distance field [41] provide an efficient representation of smooth shape for efficient simulation, we adopted as-fabricated voxel model due to the aforementioned advantages. The proposed design space provides the foundation of considering the interactions between design variables and process parameters in respect of design feasibility.

3.3 Surrogate Modeling of Design Rules. Even though design rules require less computation cost than physically based simulations, it is time-consuming to evaluate the design rules for the entire design space, which includes a huge number of design

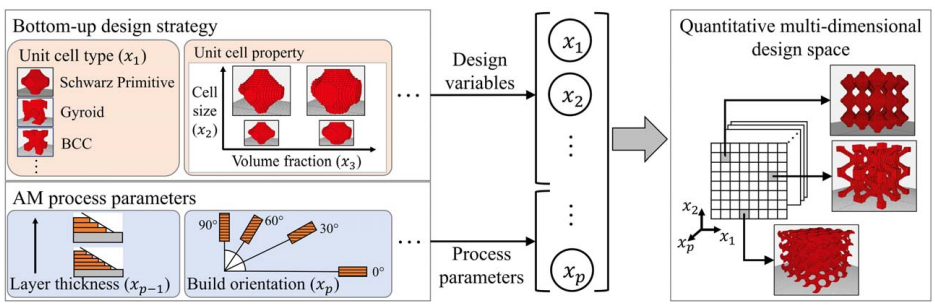

Fig. 2 The proposed quantitative design space that incorporates design variables and AM process parameters to provide the foundation of incorporating their interrelations. The design variables are provided via bottom-up design strategy.

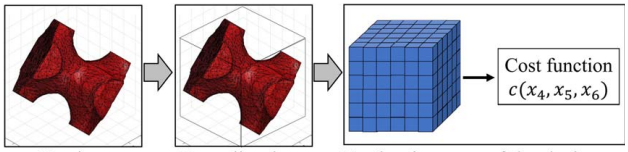

Fig. 3 The illustration of the cost function used in this case study. The cost function value is proportional to the number of voxels in the bounding box of a design.

points. For example, suppose the design space includes around 20 K of designs and the evaluation of design rules takes 3 mins in average, an exhaustive evaluation of the entire design space takes 1000 h. 1000 h may not be a big delay for the traditional product realization cycle. However, in a personalized product realization cycle where every new order yields personalized geometric design, such delays can accumulate over time on each order and thus significantly impede the design space exploration. In addition, since personalized geometric design involves complex geometric shapes, the distribution of feasibility-related features over the design space can be complex. Due to the aforementioned challenges, design space exploration in the context of personalized geometric design calls for more vigorous utilization of surrogate modeling to timely provide accurate feasible design regions.

Therefore, the objective of this step is to construct surrogate models of efficient design rules for timely identifying feasible design regions. Specifically, we first implement a set of efficient voxel model-based design rules to evaluate a subset of design points and then develop surrogate models of the design rules using the proposed cost-based experimental design. The surrogate models generate the distributions of feasibility-related features over the design space as the foundation of feasible design region identification.

3.3.1 Design Rules. Design rules can be regarded as efficient heuristics to identify the feasibility of a design, developed based on engineering knowledge, and/or learned from the experiences of domain experts. For example, for FFF process, design rules for manufacturability, which are about the feasibility-related features (e.g., minimum feature size and overhang angle), are widely adopted to quickly check the feasibility of a design. In the meantime, as-fabricated voxel model provides an efficient mechanism to implement arbitrary design rules, since such feasibility-related features can be easily derived with simple Boolean and algebraic operations enabled by voxel-based representation (e.g., estimate feature size by the number of consecutive voxels) [17]. In the context, we adopt the voxel-based implementation of rules to incorporate not only the widely adopted design rules for manufacturability (e.g., a design rule for minimum feature size) but also the domain-specific rules reflecting personalized needs (e.g., a design rule for MFC anode cavity size). The feasibility of the voxel-based implementation of design rules is demonstrated in Sec. 4.

3.3.2 Cost-Based Experimental Design. While voxel model-based design rules can be efficiently evaluated, it still takes a considerable amount of time considering that it is necessary to evaluate more than hundreds or thousands of different designs within a tight computation cost constraint. Therefore, an experimental design method is desired to minimize the design evaluation time, but at the same time, to maximize the performance of the surrogate models while satisfying a tight computation cost constraint. In this paper, we propose a cost-based experimental design, which prefers the designs with lower evaluation costs, with maintaining space-filling-ness as much as possible. Equations (1) and (2) show the proposed cost-based experimental design, which is founded upon the sequential minimum energy design (SMED) [42]. For theoretical details about the SMED, the readers are referred to the literature [42].

$$\mathbf{x}_1 = \arg\min_{\mathbf{x}} c(\mathbf{x}) \tag{1}$$

$$\mathbf{x}_{n+1} = \arg\min_{\mathbf{x}} \sum_{i=1}^{n} \frac{(c(\mathbf{x}_i)c(\mathbf{x}))^{\gamma}}{D(\mathbf{x}_i, \mathbf{x})^k} \quad \text{s.t.} \sum_{i=1}^{n+1} c(\mathbf{x}_i) \le \mathbf{C} \tag{2}$$

In Eqs. (1) and (2), $\mathbf{x}_i$ denotes the ith design point, $c(\mathbf{x})$ denotes cost function, $D(\mathbf{x}_i, \mathbf{x}_j)$ denotes Euclidean distance between the two design points, $\mathbf{C}$ denotes computation cost constraint, and γ denotes the tuning parameter to control the preference to design evaluation cost and space-filling-ness. In this paper, we choose to $k = 4p$ (where p is the dimension of the design space), which is the default value for the SMED to ensure numerical stability of the method [42]. The proposed cost-based experimental design consists of the following steps. First, the design point with the lowest evaluation cost is chosen as the initial design point, as shown in Eq. (1). If the design points with the lowest evaluation cost are not unique, initial design point is randomly chosen among them. Second, the following design points are sequentially chosen such that the potential energy, which is defined as $(c(\mathbf{x}_i)c(\mathbf{x}))^{\gamma}/D(\mathbf{x}_i, \mathbf{x})^k$ as shown in Eq. (2), is minimized. The design points are added sequentially until the total evaluation cost exceed $\mathbf{C}$.

To develop the cost-based experimental design, the following modification has been made to the SMED. First, while the SMED adopts the concept of charge function to represent the desired repulsion between the design points, the proposed method adopts the cost function $c(\mathbf{x})$, which reflects the design evaluation cost, in place of the charge function. Incorporating the cost function in the formulation of the potential energy will make in favor of the design with the lower design evaluation cost, since the potential energy is proportional to the pairwise product of cost functions of design points. Second, similar to the SMED, cost-based experimental design maximizes the distance between the design points, since the potential energy is inversely proportional to the Euclidean distance between the design points. The aforementioned properties allows the cost-based experimental design to adaptively choose design points jointly considering evaluation cost and space-filling-ness. Lastly, it should be noted that the cost-based experimental design has a tunability to be applied to a certain computation cost constraint. When $\gamma = 1/p$, the distribution of design points follows the inverse of the cost function, $1/c(\mathbf{x})$, which provides a reasonable tradeoff between space-filling-ness and design evaluation cost (For theoretical proof, the readers are referred to the literature [42]). We take $\gamma = 1/p$ as the reference value in tuning the proposed method. Given the reference value, one can tune γ to adjust the desired tradeoff between space-filling-ness and preference to the designs with lower evaluation costs. For example, for a higher γ value ($\gamma > 1/p$), the designs will only prefer the designs with extremely low design evaluation cost, which is preferable in case the computation cost constraint is extremely tight. On the other hand, for a lower γ value ($0 < \gamma < 1/p$), the designs with different evaluation costs will be similarly preferred, which can be adopted in case the computation cost constraint is relatively loose. In case, γ is extremely low, the cost-based experimental design equally favors all the designs, thus becomes almost equivalent to maximin Latin hypercube design (MmLHD), as it only maximizes the pairwise distance between the design points.

3.3.3 Surrogate Modeling. Once design points are chosen via the experimental design, the design points are used to construct surrogate models of design rules to identify the distribution of feasibility-related features. However, it should be noted that feasibility-related features have different types, either continuous or binary. For example, while minimum feature size is a continuous feature, the connectivity of anode structure is a binary feature. Therefore, based on the nature of the application, different regression methods (e.g., Gaussian process regression or regression

tree) or classification method (e.g., logistic regression or random forest) should be adopted for continuous or binary responses, respectively.

3.4 Feasible Region Identification. Given the distributions of feasibility-related features, threshold values for feasibility (based on domain knowledge) are applied to derive the distribution of binary feasibility indicators. For example, given the design rule "minimum feature size ≥2 mm," the threshold value of 2 is applied to the distribution of minimum feature size to derive the distribution of binary feasibility indicator. Then, as shown in the top-right side of Fig. 1, the distributions of different binary feasibility indicators are intersected to derive the overall feasibility distribution across the design space. In this paper, we do not consider the uncertainty of the design rules, which can be a future direction of the research.

3.4.1 Visualization of Feasible Design Region. As the design space is high-dimensional, t-distributed stochastic neighbor embedding (t-SNE) [43], which is a nonlinear dimensionality reduction technique known to recover well-separated clusters, is used to reduce the design space into a 2D space of design embeddings for visualization. Figure 4 shows an example of the visualization showing the distribution of feasible/infeasible designs in a design space for the case study in Sec. 4. Similar to exhaustive search approach, the boundary between feasible/infeasible designs can be explicitly represented, such as via the intervals of design embeddings or via visualization.

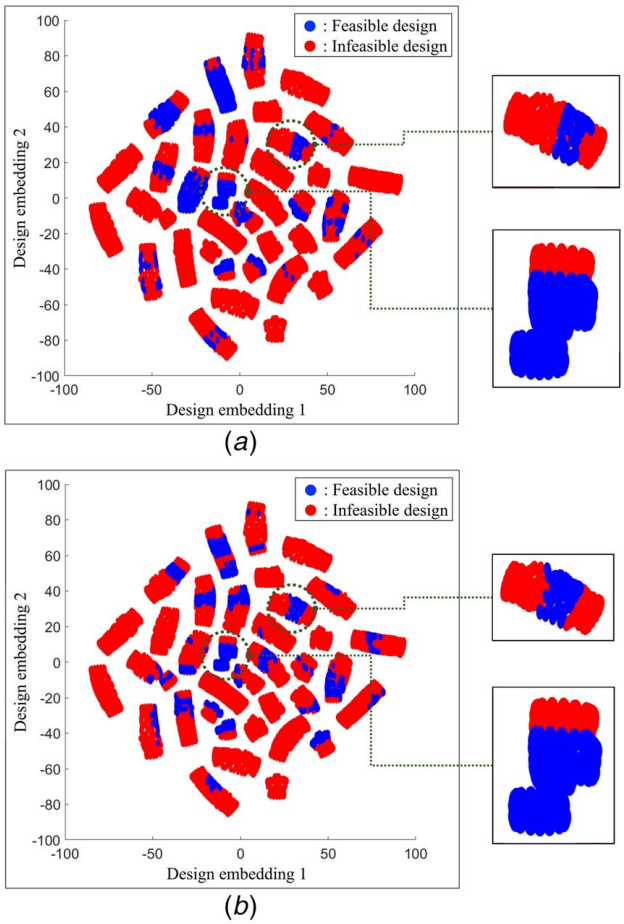

Fig. 4 Comparison of ground-truth feasible design regions and predicted results, showing the similar formation of clusters and the feasible regions within each cluster. 2% of 27,720 designs are used to generate the predicted feasible regions in Fig. 4(*b*). (*a*) Feasible design regions (ground-truth) and (*b*) feasible design regions predicted from the proposed method

3.4.2 Analysis of the Interaction Between Design Variables/Process Parameters in Design Feasibility. Once feasible design regions are identified, it is possible to investigate the quantitative relations between design variables/process parameters and design feasibility, due to the quantitative definition of the design space. Specifically, analysis of variance (ANOVA) can be performed to identify which of the design variables/process parameters interact with each other to contribute to the variation of design feasibility (i.e., the manufacturability and conformance to personalized needs). Based on the ANOVA results, it is possible to derive meaningful insight into design exploitation. For example, it is possible to identify which design variable or process parameter can be controlled to improve manufacturability without affecting the conformance to personalized needs, or vice versa.

4 Case Study: Personalized Microbial Fuel Cell Anode Design

In this section, the feasibility of the proposed method is demonstrated via the case study of personalized MFC anode design with long-term operability. It is a good test case for the proposed method due to the following reasons: (1) the design of an MFC anode is desired to be optimized for a specific target operating condition, which justifies the necessity of personalized geometric design. (2) As biochemical reaction requires a complex geometry, it justifies the use of AM, which provides great design freedom. (3) Identifying long-term operability of an MFC anode requires physically based simulations of long-term biofilm growth, which will take at least several hours per run. This justifies the use of efficient design rules for timely providing feasible design regions. In this case study, a workstation with Intel 8th gen i7 Hexa-core processor and 32 GB RAM is used to evaluate the proposed method and benchmark method.

4.1 Problem Statement and Design Space. To demonstrate the feasibility of the proposed method, we apply the method to the case study of personalized MFC anode design. The following assumptions are made for this case study.

(1) It is assumed that the size of the anode is 20 mm × 20 mm × 80 mm.
(2) The MFC operating condition is assumed to be as close as the configuration in the existing work [5].
(3) It is assumed that FFF process is used to manufacture the MFC anode.

Given the assumptions, there are 6 variables defining the design space, shown in Table 1. First, we chose TPMS-based unit cells for the anode design, since they are known to have a high surface-to-volume ratio and porosity, which are desired for a

Table 1 The list of design variables and process parameters regarding additively manufactured MFC anode design

Design variable	Type	Values chosen to define a grid over the entire design space
Unit cell type (x_1)	Categorical	"Schwarz Primitive", "Gyroid", "Schwarz Diamond", "I-WP", "OCTO", "BCC" (TPMS type unit cells)
Unit cell size (x_2)	Continuous	4, 5, 6.66, 10, 20 mm
Volume fraction control factor (x_3)	Continuous	−1.5, −1.2, −0.9, −0.6, −0.3, 0, 0.3, 0.6, 0.9, 1.2, 1.5
Layer thickness (x_4)	Continuous	0.1, 0.2, 0.3 mm
X-axis rotation (x_5)	Continuous	0, 15, 30, 45, 60, 75, 90 deg
Y-axis rotation (x_6)	Continuous	0, 15, 30, 45 deg

microbial fuel cell anode [44]. The shapes of TPMS unit cells can be defined by three design variables: unit cell type, unit cell size, and volume fraction control factor. The design variables are used to uniquely defines the overall geometric shape of the anode, specifically how the lattice structure within the geometric boundary looks like. In this case study, we assume that the unit cells are uniformly organized in the lattice structure. On the other hand, there are three process parameters provided by FFF process: layer thickness, *X*-axis rotation, and *Y*-axis rotation. The process parameters define the size of voxels, and the organization of voxels to define the geometric shape. The aforementioned six variables are used to define a grid of designs on the quantitative design space. Specifically, as shown in Table 1, the finite number of levels are chosen for each design variable and process parameter to define a multi-dimensional grid with 27,720 designs. Here, the values for x_2 are determined such that one, two, three, four, or five unit cells fit in the width of the target anode (20 mm), while the values for x_3, x_4, x_5, and x_6 are equally spaced within the lower/upper boundaries determined via observation. The 27,720 design points form the design space for experimental design, and their feasibility will be used to estimate the accuracy of feasible design regions evaluated with the proposed method. However, it should be noted that the proposed method can evaluate the feasibility of arbitrary designs (i.e., continuous values can be chosen for continuous design variables, x_2–x_6) on the design space with the surrogate models of design rules.

4.2 Design Rules. In this case study, we identified the design rules for manufacturability and MFC anode design. For the design rules about manufacturability, we choose representative rules from multiple guidelines from 3D printer manufacturers. For the design rules about MFC anode design, we reviewed the relevant literature [3–7,37] and discussed with the experts in MFC design (see Acknowledgments) to validate the design rules to be used. In total, we use four design rules, which evaluate the following feasibility-related features: minimum feature size, connectivity of the anode structure, the minimum size of anode cavities, and connectivity of the anode cavities. The first two rules are related to the manufacturability, and the latter two rules are related to the conformance to personalized needs (assuming the same operating condition to Li et al. [5]). Specifically, based on the descriptive definitions of the rules, we implemented voxel-model based implementation of the rules for this case study. The short descriptions of the design rules are as follows:

(1) Minimum feature size: For FFF process, too small feature (e.g. smaller than 2 mm) should be avoided to ensure manufacturability. This design rule counts the number of the consecutive voxels to identify minimum feature size along the horizontal plane.

(2) Connectivity of the anode structure: Connectivity of the anode structure should be guaranteed to ensure the integrity of 3d structure. This design rule checks the voxel connectivity (i.e., checking the existence of neighboring voxels) to evaluate the connectivity of the anode structure. If all the voxels are connected via other voxels, this design rule returns "True."

(3) Minimum cavity size: For MFC anode, its cavity size should not be too small to prevent clogginess during a long-term operation [5]. This design rule evaluates the size of the cavity from Euclidean distance transform of the voxel model.

(4) Connectivity of the anode cavities: Connectivity of anode cavities is desired to ensure mass transport through the anode for bio-electrochemical reactions. This design rule checks the connectivity of empty voxels (i.e., checking the existence of neighboring empty voxels) to evaluate the connectivity of anode cavities. If all the empty voxels are connected via other empty voxels, this design rule returns "True."

Table 2 The list of feasibility-related features for MFC anode and their feasible range based on domain knowledge

Design rule	Response type	Feasible range
Minimum feature size (e_1, z_1)	Continuous	>2 mm
Connectivity of the anode structure (e_2, z_2)	Binary	= True
Minimum cavity size (e_3, z_3)	Continuous	>2 mm
Connectivity of the anode cavities (e_4, z_4)	Binary	= True

Table 2 shows the list of the feasibility-related features of MFC anode based on the design rules and their feasible ranges based on domain knowledge. For the manufacturability rules, we adopted the threshold values from FFF printer manufacturers guidelines. For personalized needs for MFC anodes, we discussed with domain experts to check the validity of the rules. Design is regarded as feasible only when all the values are within the feasible range.

4.3 Surrogate Modeling and Feasible Region Identification. In this case study, the computation time of evaluating one design ranges from below 1 min to 16 min, which is shorter than a finite element analysis simulation for FFF process (more than 20 h for a single run of high-fidelity simulation [45]). However, even though the design rules provide efficient mechanisms to identify the feasibility of a design, the exhaustive evaluation of 27,720 designs takes more than 15 days. As mentioned, such delay may be accumulated to introduce a significant bottleneck in personalized product realization cycle, thus necessitate surrogate modeling to timely provide feasible design regions. In this case study, we tested the proposed design space exploration method using two different experimental designs: (1) widely adopted maximin Latin hypercube (MmLHD) as a benchmark and (2) the proposed cost-based experimental design ($\gamma = 1/p$). It should be noted that we could not compare the proposed design space exploration method with other design space exploration methods, due to the lack of physically-based simulation satisfying the tight computation cost constraint we assumed (within 10 h of computation with the test environment).

For the benchmark, we used the fixed number of design points (0.1%–2% of 27,720 designs on the grid of the design space) to generate surrogate models of feasibility-related features. For the proposed cost-based experimental design, we continued the sampling until the overall design evaluation cost reaches that of the corresponding benchmark. The cost function used in this case study is illustrated in Fig. 3. The cost function is designed based on the well-known fact that the computation cost for voxel model is proportional to the resolution of the voxel model (i.e., the number of voxels in the space) [21]. Specifically, the bounding box of a design is identified, and then the number of voxels in the bounding box is calculated to approximate the evaluation cost of the design. In this way, the cost function c depends on the parameters determining the size of bounding box and voxel, i.e., x_4 (layer thickness), x_5 (x-axis rotation), and x_6 (y-axis rotation). It should be noted that this cost function realistically reflects the actual design evaluation cost, since voxel-based design rules involve counting the number of specific voxels in the bounding box. Also, the time to derive the proposed cost function is negligible, so the evaluation of the cost function does not affect the overall design evaluation cost.

After completing the design of experiments, surrogate models of the design rules are generated to identify feasible design regions, as shown in Fig. 4. Here, design embeddings indicate the coordinates of each design point on the 2D space, which are ranged from −100 to 100, such that similar designs are stick together to form several islands in the design space. It should be noted that separated islands are formed as one of the design variables is categorical (unit cell type, x_1). As the design space is high dimensional, we

Table 3 Comparison of the number of samples evaluated within the same computation cost constraint and the performance using a benchmark method (MmLHD) vs the proposed cost-based experimental design (50 repetitions per treatment)

# of samples evaluated within the same computation cost constraint		Recall		Precision		F-measure	
Benchmark	Proposed	Benchmark	Proposed	Benchmark	Proposed	Benchmark	Proposed
28	**54**	0.307 (0.190)	**0.651 (0.158)**	0.332 (0.144)	0.319 (0.104)	0.318 (0.147)	**0.429 (0.065)**
56	**103**	0.434 (0.152)	**0.692 (0.096)**	0.493 (0.089)	0.459 (0.083)	0.458 (0.113)	**0.557 (0.060)**
112	**191**	0.561 (0.108)	**0.739 (0.084)**	0.619 (0.083)	0.543 (0.066)	0.578 (0.061)	**0.619 (0.040)**
280	**433**	0.648 (0.062)	**0.779 (0.056)**	0.699 (0.049)	0.634 (0.047)	0.669 (0.038)	**0.696 (0.024)**
560	**813**	0.688 (0.048)	**0.797 (0.039)**	0.746 (0.041)	0.722 (0.030)	0.714 (0.025)	**0.756 (0.017)**

Note: The method with larger sample size and higher Recall/F-measure are marked in bold.

used t-distributed stochastic neighbor embedding (t-SNE) [43] to visualize in a 2D space. The result demonstrates that the feasible design regions provided by the proposed method realistically represent the ground-truth with the F-measure > 0.7 (≈ 0.74). Note that only 2% of the 27,720 designs are used in producing Fig. 4(*b*). Such a visualization can be used to efficiently support the navigation of the entire design space to locate proper design candidates to be optimized. For surrogate modeling, we compared three typical regression models, linear regression, Gaussian process regression, and regression tree, as the surrogate models of design rules involving continuous feasibility-related features (i.e., e_1 and e_3 in Table 2). For surrogate models of design rules involving binary feasibility-related features (i.e., e_2 and e_4 in Table 2), we compared different classification models, including logistic regression, linear/quadratic discriminant, and random forest. Specifically, we compared every possible pair of a regression model and a classification model and then chose a pair of methods that yield the best results. In the setting of the case study, the pair of regression tree (for regression) and random forest [46] (for classification) is chosen with better performances than the other pairs. Automatically identifying a proper regression method or classification method is subject to future research direction to improve the usefulness of the proposed method.

For quantitative evaluation of the feasible design regions, we compared the feasibility/infeasibility of 27,720 designs derived via the proposed method and via exhaustive evaluation. Specifically, surrogate models are built from about 0.1%–2% of designs (training set) to predict the feasibility of the entire 27,720 designs (test set), and the predicted feasibility of the entire designs are compared with the exhaustive evaluation results. Table 3 shows evaluation results. Here, the Recall is defined as $TP/(TP+FN)$, the Precision is defined as $TP/(TP+FP)$, and the F-measure is defined as $(2 \cdot Precision \cdot Recall)/(Precision + Recall)$ where TP stands for true positive (i.e., feasible design is correctly recognized), FP stands for false positive (i.e., infeasible design is correctly recognized), and FN stands for false negative (i.e., infeasible design is wrongly recognized as feasible). In other words, Recall is the measure of how many feasible designs are correctly identified, Precision is the measure of how many designs are actually feasible assuming that they are marked as feasible, and F-measure is the measure of the overall accuracy of the result. In Table 3, the method with larger sample size and higher Recall/F-measure are marked in bold. Also, it should be noted that each row of Table 3 shares the same computation cost constraint. The results provide the following implications. First, it is shown that the proposed cost-based experimental design can utilize significantly more design points for surrogate modeling within the same computation cost constraints, as it adaptively chooses the designs with lower evaluation costs. Second, under the same computation budget, it is shown that the proposed cost-based experimental design method provides considerably higher F-measure than the benchmark method, especially when the computation cost constraints are extremely tight (i.e., low computation budget). We also observed that the proposed method shows slightly better or comparable performances when large computation budget is allowed (i.e., C in Eq. (2) is large enough), which indicates the proposed method is still acceptable in case the computation constraint is not tight. Third, even though the proposed cost-based experimental design slightly sacrifices Precision, it provides significantly higher Recall than the benchmark method. It is an important advantage since it prevents a designer from throwing away potentially better optimal designs due to the mis-classification of feasibility.

4.4 Discussion. After feasible design region identification, the entire design space is efficiently narrowed down into much smaller feasible design regions. Consequently, the efficiency of the following design exploitation can be improved, by focusing on the small feasible design regions. For example, in this case study, we observed that only 5–10% of 27,720 designs are feasible (as shown in Fig. 4), which indicates that performing design optimization without knowing the feasible design regions will lead to a considerable amount of time for burn-in to prune infeasible design candidates. It should be noted that evaluating the same number of

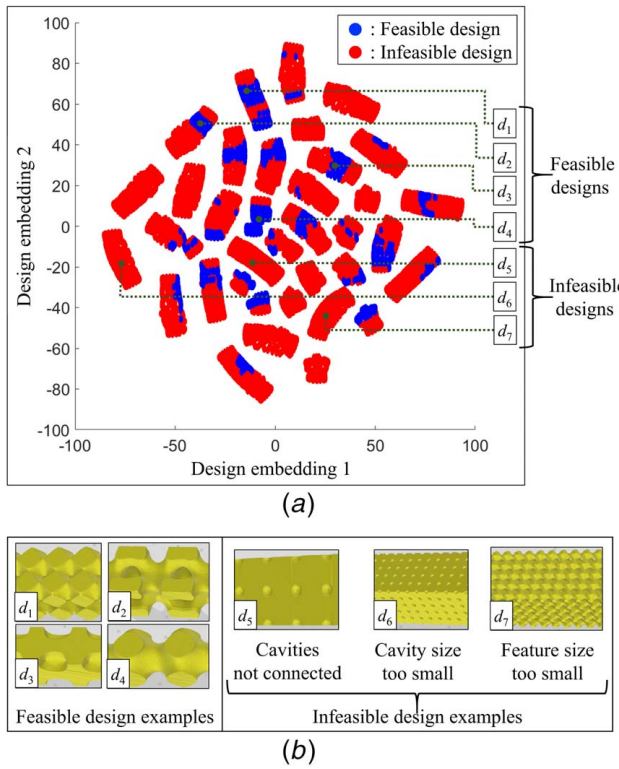

Fig. 5 Exploration of feasible and infeasible design candidates to support design exploitation in the case study. (*a*) Identification of feasible and infeasible designs from the design space via visualization and (*b*) examples of feasible and infeasible designs.

Table 4 The ANOVA results for the feasibility in terms of manufacturability (i.e., response variable: $z_1 \wedge z_2$) and conformance to personalized needs (i.e., response variable: $z_3 \wedge z_4$), when x_1 is "Schwarz Primitive" or "Gyroid"

	Unit cell type (x_1) is "Schwarz Primitive"		Unit cell type (x_1) is "Gyroid"	
Independent variables	Sum of squares (response variable: $z_1 \wedge z_2$)	Sum of squares (response variable: $z_3 \wedge z_4$)	Sum of squares (response variable: $z_1 \wedge z_2$)	Sum of squares (response variable: $z_3 \wedge z_4$)
Unit cell size (x_2)	**57.89**	**257.25**	**101.69**	5.55
Volume fraction control factor (x_3)	**720.55**	**473.32**	**666.98**	**348.13**
Layer thickness (x_4)	0.01	2.42	0.07	0.313
X-axis rotation (x_5)	1.94	2.32	15.71	**61.47**
Y-axis rotation (x_6)	1.67	3.87	16.84	6.97

Note: The values indicating considerable contribution to the feasibility are marked in bold font.

design points with physically based computer simulations is prohibitive, especially in case multi-physics simulations are involved, since they cannot evaluate enough number of design point within a tight computation cost constraint (10 h of computation, in this case study). Specifically, for this case study, it is necessary to simulate the biofilm build-up on the MFC anode surface, which is expected to take at least several hours for each run [11].

In addition, for personalized product realization where a large number of different requirements should be addressed (i.e., computation cost constraint becomes much tighter), the proposed experimental design will provide more feasible design regions with higher Recall than typical space-filling designs, as it allows the evaluation of more samples for surrogate modeling. Also, the proposed cost-based experimental design can satisfy an arbitrary computation cost constraint by sequentially adding design points until the total design evaluation cost exceeds the computation cost constraint.

Furthermore, the proposed method can provide insightful information and visualization to facilitate design exploitation. First, it provides a small feasible design region over the entire design space, such that a designer can better identify different characteristics of feasible/infeasible designs and locate proper design candidates. Figure 5 shows the examples of feasible and infeasible design candidates on the design space explored in the case study. A designer can explore feasible designs, such as d_1, d_2, d_3, and d_4 shown in Fig. 5, and identify distinct feasible designs, which provide good starting points to identify different local optimal designs during design optimization. Similarly, a designer can explore infeasible designs, such as d_5, d_6, and d_7 shown in Fig. 5, and understand the distribution of different infeasible designs based on their issues (e.g., too small cavity). Combined with design candidate identification support system [47] in the literature, the proposed method can improve the effectiveness of identifying proper design candidates and their optimization. The proposed method can also help a designer to address an extreme case in the design candidate identification. For example, in the case that the feasible design region is too small, or there is no feasible design region, one can extend the boundaries of the design space and/or relax the design rules to guide the design candidate identification. Second, the proposed quantitative design space provides the capability to identify how design variables/process parameters interact and contribute to the variation of the design feasibility (i.e., the manufacturability and conformance to personalized needs). Specifically, based on the analysis of variance (ANOVA) results, we found out that for different cell types (x_1), different variables may contribute to the variance of the manufacturability (i.e., $z_1 \wedge z_2$) or conformance to personalized needs (i.e., $z_1 \wedge z_2$), as shown in Table 4.

For example, for the cell type of "Schwarz Primitive," cell size (x_2) and volume fraction (x_3) most contribute to the variance of both manufacturability and conformance to personalized needs. On the other hand, for the cell type of "Gyroid," while cell size (x_2) and volume fraction (x_3) most contribute to the variance of the manufacturability, volume fraction (x_3) and *x*-axis rotation (x_5) most contribute to the variance of the conformance to personalized needs. The result implies that when the unit cell type is "Gyroid," it is possible to control the manufacturability or conformance to personalized needs without much impact on the other type of feasibility.

While this case study is performed upon the three assumptions (i.e., MFC anode size, operating condition, and manufacturing process are specified), the proposed method can be easily applied to different scenario of personalized MFC anode design. First, it can be applied to design different sizes of MFC anode by adjusting the overall size of the design during the generation of lattice structure. Second, for different operating condition or different manufacturing process, design rules can be modified based on the relevant literature. For example, the rules related to the conformance to personalized needs for MFC anode can be adjusted based on the relevant literature assuming different operating conditions [3,4,6,7,37], and the design rules related to the manufacturability can be replaced to those of different manufacturing process, such as stereolithography [22]. The proposed method can be widely adopted to design different types of products where adopting a lattice structure is beneficial, and relevant design rules are available. For example, the proposed method can be applied to personalized prosthetic hand design, by using manufacturability rules on stereolithograpy [22] and dimensioning/selection rules on prosthesis design [23,24]. The acquisition of such design rules can be efficiently done by the advancement of automated frameworks for rule extraction from text [27].

5 Conclusion

In this paper, we propose a cost-efficient data-driven design exploration method for personalized geometric design, founded on the quantitative design space provide by the bottom-up design strategy. Specifically, the method relies on the surrogate models of efficient voxel model-based design rules to timely deliver feasible design regions, which is extremely challenging with the existing methods relying on physically based computer simulations. Also, we propose the cost-based experimental design method to construct more precise surrogate models within a tight computation cost constraint to meet the constraint for streamlining personalized product realization. We verified the feasibility of the proposed design space exploration method via the case study of personalized MFC anode design, and demonstrated the advantages of the proposed cost-based experimental design.

The proposed method has four contributions in terms of efficient design space exploration for the personalized product realization in AM. First, the proposed method provides a quantitative design space and feasible design regions for the personalized geometric design for AM. Therefore, it provides the foundation of quantitatively identifying the important interactions between design variables/process parameters how they contribute to design feasibility (i.e., the manufacturability and conformance to personalized needs). We expect that this will provide important insight to improve the design exploitation followed by design space exploration. Second, the proposed method provides a systematic mechanism to implement domain

knowledge for efficient design space exploration. This method resembles the way that domain experts rely on their insight to quickly filter out infeasible designs. In a similar manner, the proposed method efficiently provides tailored feasible design region to facilitate the follow-up design exploitation (e.g., more detailed simulation-based exploration or design optimization) in the personalized product realization. Third, when the computation cost constraint for design space exploration is tight, the proposed cost-based experimental design provides significantly better results than using a typical space-filling design, thus contribute to streamlining the personalized product realization. Lastly, the proposed method can be easily extended to a wide variety of applications and AM processes by adopting domain knowledge for the target domain. For example, as layer-wise AM processes share similar design rules, the case study provided in this paper can be applied to selective laser sintering and stereolithography without much modifications. Also, with the advancement of rule extraction technologies, the proposed method can be applied to completely different domains if relevant design rules are accessible. For example, design rules can be extracted from a standard specification of printed electronics [25] to guide personalized foldable/rollable electronics design [26]. Further extension of the proposed method is possible when design rules are available. For example, the proposed method can be extended to the personalized geometric design of a lightweight prosthesis, based on the design rules on stereolithography [22] and the design rules (e.g., sizing, dimensioning, and selection rules) on prosthesis [23,24]. In conclusion, the proposed method can contribute to addressing the design bottleneck and streamlining the personalized product realization cycle adapting to faster-changing markets.

Although we have made contributions to the research area of design space exploration for personalized geometric design for AM, we believe the following further investigations can contribute to the broader acceptance of the proposed method. First, improving the proposed bottom-up design strategy to be applicable to conformal lattice structure [48] is desired. This will allow the method to be applicable to a wide variety of practical product designs. Second, the proposed method is founded upon the assumption that reliable design rules are available and a design is feasible when it satisfies all the design rules. However, quantifying the uncertainty of design rules and the association between them (i.e., relative weights of design rules in deciding design feasibility, and its sensitivity analysis) need to be investigated. This will allow the proposed method to consider heterogeneous capabilities of different AM machines, likely to occur under a collaborative manufacturing scenario [49], where the generic design rules need to be tuned to precisely identify design feasibility. Third, the current work used the voxel as small as $0.1\ \text{mm} \times 0.1\ \text{mm} \times 0.1\ \text{mm}$ (depending on layer thickness). It needs further investigation on how to extend the proposed method for allowing sub-voxel geometric variation, such as due to the variation of feed rate and extruder temperature, different material properties, and/or diffusion of material [50]. Such an extension will enable the incorporation of non-geometric process setting parameters (e.g., material type and extruder temperature), as well as significantly improve the flexibility and accuracy of the proposed method especially when a design rule involves extremely small threshold value.

Acknowledgment

The authors acknowledge Dr. Zhen (Jason) He (Department of Energy, Environmental & Chemical Engineering, Washington University in St. Louis) and his student Mr. Zixuan Wang for their comments on MFC anode structure design strategy, their support on the identification of relevant design rules.

Conflict of Interest

There are no conflicts of interest.

Data Availability Statement

The datasets generated and supporting the findings of this article are obtainable from the corresponding author upon reasonable request.

References

[1] Tofail, S. A., Koumoulos, E. P., Bandyopadhyay, A., Bose, S., O'Donoghue, L., and Charitidis, C., 2018, "Additive Manufacturing: Scientific and Technological Challenges, Market Uptake and Opportunities," Mater. Today, **21**(1), pp. 22–37.
[2] Li, W.-W., Yu, H.-Q., and He, Z., 2014, "Towards Sustainable Wastewater Treatment by Using Microbial Fuel Cells-centered Technologies," Energy Environ. Sci., **7**(3), pp. 911–924.
[3] Logan, B. E., Hamelers, B., Rozendal, R., Schröder, U., Keller, J., Freguia, S., Aelterman, P., Verstraete, W., and Rabaey, K., 2006, "Microbial Fuel Cells: Methodology and Technology," Environ. Sci. Technol., **40**(17), pp. 5181–5192.
[4] Santoro, C., Arbizzani, C., Erable, B., and Ieropoulos, I., 2017, "Microbial Fuel Cells: From Fundamentals to Applications. A Review," J. Power. Sources., **356**, pp. 225–244.
[5] Li, J., Zhang, J., Ye, D., Zhu, X., Liao, Q., and Zheng, J., 2014, "Optimization of Inner Diameter of Tubular Bamboo Charcoal Anode for a Microbial Fuel Cell," Int. J. Hydrogen Energy, **39**(33), pp. 19242–19248.
[6] Guo, K., Prévoteau, A., Patil, S. A., and Rabaey, K., 2015, "Engineering Electrodes for Microbial Electrocatalysis," Curr. Opin. Biotechnol., **33**, pp. 149–156.
[7] You, J., Preen, R. J., Bull, L., Greenman, J., and Ieropoulos, I., 2017, "3d Printed Components of Microbial Fuel Cells: Towards Monolithic Microbial Fuel Cell Fabrication Using Additive Layer Manufacturing," Sustain. Energy Technol. Assessments, **19**, pp. 94–101.
[8] Strack, G., 2019, "Additive Manufacturing Approaches for Biological Power Generation," Current Opinion Electrochem., **17**, pp. 167–173.
[9] Jared, B. H., Aguilo, M. A., Beghini, L. L., Boyce, B. L., Clark, B. W., Cook, A., Kaehr, B. J., and Robbins, J., 2017, "Additive Manufacturing: Toward Holistic Design," Scr. Mater., **135**, pp. 141–147.
[10] Leung, Y.-S., Kwok, T.-H., Li, X., Yang, Y., Wang, C. C., and Chen, Y., 2019, "Challenges and Status on Design and Computation for Emerging Additive Manufacturing Technologies," ASME J. Comput. Inf. Sci. Eng., **19**(2), p. 021013.
[11] Ortiz-Martínez, V., Salar-García, M., De Los Ríos, A., Hernández-Fernández, F., Egea, J., and Lozano, L., 2015, "Developments in Microbial Fuel Cell Modeling," Chem. Eng. J., **271**, pp. 50–60.
[12] Sigmund, O., and Maute, K., 2013, "Topology Optimization Approaches," Struct. Multidiscipl. Optim., **48**(6), pp. 1031–1055.
[13] van Dijk, N. P., Maute, K., Langelaar, M., and Van Keulen, F., 2013, "Level-set Methods for Structural Topology Optimization: A Review," Struct. Multidiscipl. Optim., **48**(3), pp. 437–472.
[14] Deaton, J. D., and Grandhi, R. V., 2014, "A Survey of Structural and Multidisciplinary Continuum Topology Optimization: Post 2000," Struct. Multidiscipl. Optim., **49**(1), pp. 1–38.
[15] Dbouk, T., 2017, "A Review About the Engineering Design of Optimal Heat Transfer Systems Using Topology Optimization," Appl. Therm. Eng., **112**, pp. 841–854.
[16] Martínez, J., Dumas, J., and Lefebvre, S., 2016, "Procedural Voronoi Foams for Additive Manufacturing," ACM Trans. Graph. (TOG), **35**(4), pp. 1–12.
[17] Lynn, R., Saldana, C., Kurfess, T., Reddy, N., Simpson, T., Jablokow, K., Tucker, T., Tedia, S., and Williams, C., 2016, "Toward Rapid Manufacturability Analysis Tools for Engineering Design Education," Proc. Manufact., **5**, pp. 1183–1196.
[18] Shi, Y., Zhang, Y., Baek, S., De Backer, W., and Harik, R., 2018, "Manufacturability Analysis for Additive Manufacturing Using a Novel Feature Recognition Technique," Comput.-Aided Des. Appl., **15**(6), pp. 941–952.
[19] Morris, C., Bekker, L., Haberman, M. R., and Seepersad, C. C., 2018, "Design Exploration of Reliably Manufacturable Materials and Structures with Applications to Negative Stiffness Metamaterials and Microstereolithography," ASME J. Mech. Des., **140**(11), p. 111415.
[20] Xiong, Y., Duong, P. L. T., Wang, D., Park, S.-I., Ge, Q., Raghavan, N., and Rosen, D. W., 2019, "Data-driven Design Space Exploration and Exploitation for Design for Additive Manufacturing," ASME J. Mech. Des., **141**(10), p. 101101.
[21] Park, S.-i., and Rosen, D. W., 2016, "Quantifying Effects of Material Extrusion Additive Manufacturing Process on Mechanical Properties of Lattice Structures Using As-fabricated Voxel Modeling," Addit. Manuf., **12**, pp. 265–273.
[22] Pham, D., and Ji, C., 2000, "Design for Stereolithography," Proc. Inst. Mech. Engin. Part C: J. Mech. Engin. Sci., **214**(5), pp. 635–640.
[23] Colombo, G., Facoetti, G., and Rizzi, C., 2013, "A Digital Patient for Computer-aided Prosthesis Design," Interface Focus, **3**(2), p. 20120082.
[24] Belter, J. T., Segil, J. L., Dollar, A. M., and Weir, R. F., 2013, "Mechanical Design and Performance Specifications of Anthropomorphic Prosthetic Hands: a Review," J. Rehab. Res. Develop., **50**(5), pp. 599–618.
[25] Hodgson, A., 2013, "Iec Tc119–international Standards for Printed Electronics," NIP29: 29th International Conference on Digital Printing Technologies, Vol. 2013, Seattle, WA, Society for Imaging Science and Technology, pp. 369–371.
[26] Yang, Y., and Gao, W., 2019, "Wearable and Flexible Electronics for Continuous Molecular Monitoring," Chem. Soc. Rev., **48**(6), pp. 1465–1491.

[27] Kang, S., Patil, L., Rangarajan, A., Moitra, A., Robinson, D., Jia, T., and Dutta, D., 2019, "Ontology-Based Ambiguity Resolution of Manufacturing Text for Formal Rule Extraction," ASME J. Comput. Inf. Sci. Eng., **19**(2), p. 021003.
[28] Olewnik, A., Brauen, T., Ferguson, S., and Lewis, K., 2004, "A Framework for Flexible Systems and Its Implementation in Multiattribute Decision Making," ASME J. Mech. Des., **126**(3), pp. 412–419.
[29] Gurnani, A., Ferguson, S., Lewis, K., and Donndelinger, J., 2006, "A Constraint-based Approach to Feasibility Assessment in Preliminary Design," AI EDAM, **20**(4), pp. 351–367.
[30] Siddiqi, A., and de Weck, O. L., 2008, "Modeling Methods and Conceptual Design Principles for Reconfigurable Systems," ASME J. Mech. Des., **130**(10), p. 101102.
[31] Pate, D. J., Patterson, M. D., and German, B. J., 2012, "Optimizing Families of Reconfigurable Aircraft for Multiple Missions," J. Aircraft, **49**(6), pp. 1988–2000.
[32] Choi, H., McDowell, D. L., Allen, J. K., Rosen, D., and Mistree, F., 2008, "An Inductive Design Exploration Method for Robust Multiscale Materials Design," ASME J. Mech. Des., **130**(3), p. 031402.
[33] Matthews, J., Klatt, T., Morris, C., Seepersad, C. C., Haberman, M., and Shahan, D., 2016, "Hierarchical Design of Negative Stiffness Metamaterials Using a Bayesian Network Classifier," ASME J. Mech. Des., **138**(4), p. 041404.
[34] Shahan, D. W., and Seepersad, C. C., 2012, "Bayesian Network Classifiers for Set-based Collaborative Design," ASME J. Mech. Des., **134**(7), p. 071001.
[35] Chen, W., and Fuge, M., 2017, "Beyond the Known: Detecting Novel Feasible Domains Over An Unbounded Design Space," ASME J. Mech. Des., **139**(11), p. 111405.
[36] Rosen, D. W., 2014, "Research Supporting Principles for Design for Additive Manufacturing: This Paper Provides a Comprehensive Review on Current Design Principles and Strategies for Am," Virtual Phys. Prototyping, **9**(4), pp. 225–232.
[37] Calignano, F., Tommasi, T., Manfredi, D., and Chiolerio, A., 2015, "Additive Manufacturing of a Microbial Fuel Cell'a Detailed Study," Sci. Rep., **5**, p. 17373.
[38] Maskery, I., Aremu, A., Parry, L., Wildman, R., Tuck, C., and Ashcroft, I., 2018, "Effective Design and Simulation of Surface-Based Lattice Structures Featuring Volume Fraction and Cell Type Grading," Mater. Des., **155**, pp. 220–232.
[39] Chang, P. S., and Rosen, D. W., 2013, "The Size Matching and Scaling Method: a Synthesis Method for the Design of Mesoscale Cellular Structures," Int. J. Comput. Integr. Manufact., **26**(10), pp. 907–927.
[40] Chandru, V., Manohar, S., and Prakash, C. E., 1995, "Voxel-based Modeling for Layered Manufacturing," IEEE Comput. Graph. Appl., **15**(6), pp. 42–47.
[41] Barclay, J., Dhokia, V., and Nassehi, A., 2016, "Additive Manufacturing Simulation Using Signed Distance Fields," International Conference on Sustainable Design and Manufacturing, Heraklion, Greece, Apr. 4–6, Springer, pp. 435–444.
[42] Joseph, V. R., Dasgupta, T., Tuo, R., and Wu, C. J., 2015, "Sequential Exploration of Complex Surfaces Using Minimum Energy Designs," Technometrics, **57**(1), pp. 64–74.
[43] Maaten, L. v. d., and Hinton, G., 2008, "Visualizing Data Using T-sne," J. Mach. Learn. Res., **9**(Nov), pp. 2579–2605.
[44] You, J., Fan, H., Winfield, J., and Ieropoulos, I. A., 2020, "Complete Microbial Fuel Cell Fabrication Using Additive Layer Manufacturing," Molecules, **25**(13), p. 3051.
[45] Li, J., Jin, R., and Hang, Z. Y., 2018, "Integration of Physically-Based and Data-Driven Approaches for Thermal Field Prediction in Additive Manufacturing," Mater. Des., **139**, pp. 473–485.
[46] Breiman, L., 2001, "Random Forests," Mach. Learn., **45**(1), pp. 5–32.
[47] Yang, S., Page, T., Zhang, Y., and Zhao, Y. F., 2020, "Towards An Automated Decision Support System for the Identification of Additive Manufacturing Part Candidates," J. Intel. Manufact., **31**(8), 1–17.
[48] Aremu, A. O., Brennan-Craddock, J., Panesar, A., Ashcroft, I., Hague, R. J., Wildman, R. D., and Tuck, C., 2017, "A Voxel-Based Method of Constructing and Skinning Conformal and Functionally Graded Lattice Structures Suitable for Additive Manufacturing," Addit. Manuf., **13**, pp. 1–13.
[49] Wang, J., Xu, C., Zhang, J., Bao, J., and Zhong, R., 2020, "A Collaborative Architecture of the Industrial Internet Platform for Manufacturing Systems," Robot. Comput.-Integr. Manufact., **61**, p. 101854.
[50] Ueng, S.-K., Chen, L.-G., and Jen, S.-Y., 2018, "Voxel-Based Virtual Manufacturing Simulation for Three-Dimensional Printing," Adv. Mech. Engin., **10**(6), pp. 1–14.